THE JOURNAL OF BIOLOGICAL CHEMISTRY VOL. 286, NO. 13, pp. 11672–11684, April 1, 2011

Dynamic Regulation of the Mitochondrial Proton Gradient during Cytosolic Calcium Elevations*[S]

Received for publication, July 1, 2010, and in revised form, January 10, 2011 Published, JBC Papers in Press, January 11, 2011, DOI 10.1074/jbc.M110.159962

Damon Poburko[1], **Jaime Santo-Domingo, and Nicolas Demaurex**[2]

From the Department of Cell Physiology and Metabolism, University of Geneva Medical School, 1 Michel-Servet, CH-1211 Geneva 4, Switzerland

Mitochondria extrude protons across their inner membrane to generate the mitochondrial membrane potential ($\Delta\Psi_m$) and pH gradient (ΔpH_m) that both power ATP synthesis. Mitochondrial uptake and efflux of many ions and metabolites are driven exclusively by ΔpH_m, whose *in situ* regulation is poorly characterized. Here, we report the first dynamic measurements of ΔpH_m in living cells, using a mitochondrially targeted, pH-sensitive YFP (SypHer) combined with a cytosolic pH indicator (5-(and 6)-carboxy-SNARF-1). The resting matrix pH (~7.6) and ΔpH_m (~0.45) of HeLa cells at 37 °C were lower than previously reported. Unexpectedly, mitochondrial pH and ΔpH_m decreased during cytosolic Ca^{2+} elevations. The drop in matrix pH was due to cytosolic acid generated by plasma membrane Ca^{2+}-ATPases and transmitted to mitochondria by P_i/H^+ symport and K^+/H^+ exchange, whereas the decrease in ΔpH_m reflected the low H^+-buffering power of mitochondria (~5 mM, pH 7.8) compared with the cytosol (~20 mM, pH 7.4). Upon agonist washout and restoration of cytosolic Ca^{2+} and pH, mitochondria alkalinized and ΔpH_m increased. In permeabilized cells, a decrease in bath pH from 7.4 to 7.2 rapidly decreased mitochondrial pH, whereas the addition of 10 μM Ca^{2+} caused a delayed and smaller alkalinization. These findings indicate that the mitochondrial matrix pH and ΔpH_m are regulated by opposing Ca^{2+}-dependent processes of stimulated mitochondrial respiration and cytosolic acidification.

Mitochondria are mobile intracellular integrators of metabolic and ionic signaling. These multifunctional organelles generate ATP by oxidative phosphorylation, integrate signaling cascades leading to the release of proapoptotic factors (1), and shape cellular Ca^{2+} signals by taking up and releasing Ca^{2+} ions (2). By acting as transient Ca^{2+} buffers, mitochondria alter the propagation of Ca^{2+} waves, modulate the activity of plasma membrane channels and transporters (3, 4), and facilitate the refilling of intracellular Ca^{2+} stores (5, 6) (reviewed in Ref. 7). Mitochondrial metabolism and intracellular Ca^{2+} signaling are closely linked. Increases in the free Ca^{2+} concentration in the mitochondrial matrix ($[Ca^{2+}]_{mit}$)[3] activate mitochondrial dehydrogenases to stimulate oxidative phosphorylation (8), and Ca^{2+} elevations in the intermembrane space stimulate the uptake of substrates of oxidative phosphorylation (9, 10). Moreover, electrophoretic Ca^{2+} uptake into the matrix is thought to reduce the electrical resistance for pumping protons out of the matrix (11).

Mitochondria are double membrane organelles with an outer membrane permeable to solutes and an inner membrane harboring the respiratory chain complexes. The respiratory chain extrudes protons from the mitochondrial matrix into the intermembrane space to generate a maximal proton-motive force ($\Delta\tilde{\mu}_{H^+}$) of ~220 mV across the inner mitochondrial membrane (12). The $\Delta\tilde{\mu}_{H^+}$ is the sum of the electrical potential across the inner membrane ($\Delta\Psi_m$, negative inside) and the pH gradient between the bulk solutions on either side of the membrane (ΔpH_m, alkaline inside). According to Mitchell's chemiosmotic theory, $\Delta\Psi_m$ and ΔpH_m are thermodynamically equivalent driving forces for the synthesis of ATP by F_1F_0 ATP-synthase (13) (reviewed in Ref. 14). Recent studies, however, indicate that ATP synthesis by purified F_0 complexes reconstituted in liposomes requires a high concentration of protons (pH <6.5) at the source P site of the enzyme (15) (reviewed in Ref. 16). Efficient ATP synthesis thus require not only a high driving force for protons but also a low pH within the cristae of mitochondria. These data imply that a ΔpH_m of >1 pH unit must be maintained to enable the synthesis of ATP by respiring mitochondria.

The mitochondrial pH gradient (ΔpH_m) is the sole driving force for the electroneutral transport of many ions and metabolites in and out of the mitochondrial matrix, whereas the activity of several mitochondrial ion exchangers is coupled, directly or indirectly, to the electroneutral movement of protons (17). For instance, the mitochondrial Na^+ gradient is clamped close to ΔpH_m by the electro-neutral mitochondrial $1Na^+:1H^+$ exchanger (mNHE) (reviewed in Ref. 7). The sodium gradient, in turn, drives electrogenic mitochondrial $1Ca^+:3Na^+$ exchange (18) by the recently identified protein NCLX (19) that regulates mitochondrial Ca^{2+} levels. Electroneutral K^+/H^+ exchange catalyzed by the protein Letm1 is essential for mito-

* This work was supported in part by Swiss National Foundation Grant 31-068317 (to N. D.).

⌘ *Author's Choice*—Final version full access.

[S] The on-line version of this article (available at http://www.jbc.org) contains supplemental Figs. S1–S6.

[1] Supported in part by the Canadian Natural Sciences and Engineering Research Council.

[2] To whom correspondence should be addressed. Tel.: 41-22-379-5399; Fax: 41-22-379-5338; E-mail: Nicolas.Demaurex@unige.ch.

[3] The abbreviations used are: $[Ca^{2+}]_{mit}$, mitochondrial free ionic Ca^{2+}; mNHE, mitochondrial $1Na^+:1H^+$ exchanger; 2-APB, 2-aminoethoxyl diphenylborate; NCX, Na^+/Ca^{2+} exchanger; mNCX, mitochondrial NCX; pH_{cyt}, cytosolic pH; pH_{mito}, mitochondrial matrix pH; ΔpH_m, mitochondrial pH gradient; PMCA, plasma membrane Ca^{2+} ATPase; SERCA, sarco/endoplasmic reticulum Ca^{2+} ATPase; ETC, electron transport chain; SNARF, 5-(and 6)-carboxy-SNARF-1.

chondrial ionic and volume homeostasis (20, 21). The Letm1 protein was recently proposed to be an electrogenic Ca^{2+}/H^+ antiporter with a 1:1 stoichiometry (22), despite earlier studies indicating that Ca^{2+} enters mitochondria as the fully charged species (23–25) and exits mitochondria with a $3H^+$:$1Ca^{2+}$ stoichiometry (26). Regardless of whether Letm1 transports K^+ or Ca^{2+} in exchange for H^+, its exchange activity depends on ΔpH_m. Finally, ΔpH_m also influences the amplitude of $[Ca^{2+}]_{mit}$ elevations in that the mitochondrial Ca^{2+}-buffering power is determined by the mitochondrial phosphate concentration, which is modulated by ΔpH_m (27). Mitochondria therefore rely on ΔpH_m to generate ATP, to move ions and metabolites, and to buffer Ca^{2+} ions.

The regulation of $\Delta\tilde{\mu}_{H^+}$ has been extensively studied because it is essential for oxidative phosphorylation. Early approaches to estimate $\Delta\tilde{\mu}_{H^+}$ in isolated mitochondria used potassium- and proton-selective electrodes or isotopes to detect changes in the external concentration of these ions in the presence of the K^+ ionophore valinomycin to provide a diffusion potential (12, 28). These experiments revealed that at low external K^+ concentrations, ΔpH_m contributes up to 170 mV to the proton-motive force (12). In physiological conditions, however (*i.e.* high K^+ concentrations and no valinomycin), the situation is reversed, and $\Delta\Psi_m$ contributes most of the proton-motive force. These findings were validated by subsequent determinations of $\Delta\Psi_m$ in isolated mitochondria and intact cells with fluorescent lipophilic cations (reviewed in Ref. 29). Our current knowledge of ΔpH_m regulation is largely based on early experiments in isolated mitochondria that employed minimal sucrose buffers and H^+/K^+ ionophores, such as nigericin (30, 31). In intact cells, ΔpH_m has been estimated around 1.0–1.2 pH units by isotopic measurements of weak acid or bases (32, 33), thus contributing ~60 mV to $\Delta\tilde{\mu}_{H^+}$. More recent studies using fluorescent indicators yielded ΔpH_m values of 0.5–0.9 pH units based on separate static measurements of matrix, cytosolic or inter-membrane space pH in sister cultures of live cells (34). These studies brought us closer to direct measurement of ΔpH_m in live cells but were unable to resolve the dynamic regulation of ΔpH_m by factors like Ca^{2+} uptake, the activity of the mitochondrial permeability transition pore (35), and the presence of uncoupling proteins (36).

In this study, we simultaneously measured cytosolic pH using the well characterized dye 5-(and 6)-carboxy-SNARF-1 (SNARF) and matrix pH using a ratiometric circularly permuted YFP. The concurrent measurements of pH in the cytosol (pH_{cyto}) and mitochondrial matrix (pH_{mito}) provided real-time measurement of the cytosol-matrix pH gradient, and thus of ΔpH_m, in intact cells. Moreover, this approach enabled us to determine the proton-buffering power of the matrix of intact mitochondria. Unexpectedly, we observed that $[Ca^{2+}]_{cyt}$ elevations were associated with massive cytosolic and matrix pH decreases and consequent decreases in ΔpH_m.

EXPERIMENTAL PROCEDURES

Reagents—Minimum essential medium with Glutamax (catalog no. 41090), fetal calf serum, penicillin/streptomycin, Lipofectamine 2000, SNARF/AM (C1272), and Fura-2 (F1201) were from Invitrogen. Histamine, 2-APB, orthovanadate, nigericin, monensin, antimycin, oligomycin, and rotenone were from Sigma. Transfast was from Promega. The QuikChange II site-directed mutagenesis kit was from Stratagene. Mutagenesis primers were from Microsynth (Balgach, Switzerland). HyPer plasmids were from Evrogen (Moscow, Russia). $YC3.6_{cyto}$ and 4mitD3-CPV were kindly provided by Drs. Amy Palmer and Roger Tsien.

Cell Culture and Transfection—Culturing of HeLa cells was described previously (37). For epifluorescence microscopy, cells were plated on 25-mm glass coverslips in 35-mm culture dishes. For high throughput experiments, 5000–8000 cells/well were plated on clear bottom, black-walled 96-well plates (catalog no. 655090, Greiner Bio One). Coverslips were transfected with 2 μg of DNA and Lipofectamine 2000 (4 μl) or Transfast (3.5 μl) as per the manufacturer's instructions. Cells on 96-well plates were treated with 1.1 μl of Lipofectamine 2000 and 0.4 μg of DNA in 200 μl of medium/well for 6–24 h and imaged 2 days later.

Cell Permeabilization—MitoSypHer-expressing HeLa cells were permeabilized on the microscope with a 1-min exposure to digitonin (100 μM) in Ca^{2+}-free intracellular buffer: 120 mM KCl, 10 mM NaCl, 1 mM H_2KPO_4, 20 mM HEPES, 5 mM succinic acid, 1 mM ATP-Mg^{2+}, 0.02 mM ADP-K, 1 mM $MgCl_2$ (1 mM Mg^{2+}-free), 0.5 mM EGTA adjusted to pH 7.4 with KOH. After digitonin washout, pH was stepped between 7.4 and 7.2 by turnover of the bath solution. The addition of Ca^{2+} or drugs was performed by full bath turnover. Total $CaCl_2$ and $MgCl_2$ was 0.327 and 5.5 mM, respectively, at pH 7.4, and 0.326–5.43 mM at pH 7.2 to give ~10 μM free Ca^{2+} buffered with 5 mM HEDTA and 1 mM ATP-Mg^{2+} as calculated with Max Chelator.

Conversion of HyPer to SypHer—In their description of HyPer, Belousov *et al.* (38) noted that mutation of either of two H_2O_2-sensing cysteine residues to a serine caused total loss of HyPer sensitivity to H_2O_2. We mutated the first cysteine in cytosolic and mitochondria-targeted HyPer to make SypHer. Briefly, the C199S mutation was performed with the QuikChange II site-directed mutagenesis kit as per the manufacturer's instructions using 12 reaction cycles with 5.5 min for elongation in each. Primers were used at 10-fold the suggested concentration, and primers were 5′-agatggtcactctttgcgcgat-3′ (forward) and 5′-atcgcgcaaagagtgaccatct-3′ (reverse),[4] with underlined nucleotides showing the position of the point mutation. PCRs were transformed into XL1-blue bacteria, and minipreps (Gene Elute, Sigma) were prepared from clonal colonies for sequencing to confirm the C199S mutation and the absence of other mutations. Mutated plasmids were transfected into HeLa cells to confirm their sensitivity of pH and lack of response to H_2O_2 (200 μM).

pH Measurements—Experiments were performed in HEPES buffer (HBSS) solution containing 140 mM NaCl, 5 mM KCl, 1 mM $MgCl_2$, 2 mM $CaCl_2$, 20 mM Hepes, 10 mM glucose, pH set to 7.4 with NaOH at 37 °C. Ca^{2+}-free solution contained 0.2 mM EGTA instead of $CaCl_2$. Cells grown on glass coverslips were inserted into a thermostatic chamber (Harvard Apparatus, Holliston, MA), and solutions were changed by hand. Ratiometric

[4] Dr. Vsevolod Belousov, personal communication.

pH and Ca^{2+} images were acquired with a ×40 objective (1.3 numerical aperture, Zeiss Axiovert s100TV) and a cooled CCD camera (MicroMax, Roper Scientific) (37). For pH imaging, SypHer (cytosolic or mitochondrial) was alternately excited for 200–300 ms at 430 and 480 nm through a 505DCXR dichroic filter and imaged with a 535DF25 band pass filter (Omega Optical). For simultaneous mitochondrial/cytosolic pH measurements, SypHer-expressing cells were loaded with SNARF (5 μM, 0.2% DMSO, 0.01% pluronic F-127, 30 min, ambient temperature) followed by 20 min of de-esterification before 10 min of equilibration on the heated stage. SypHer was imaged as above, and SNARF was excited at 480 nm for 200 ms through the same dichroic filter and imaged with 580DF30 and 640DF35 filters (Omega Optical). Image pairs and quartets were typically acquired every 2–5 s. Fluorescence ratios (F480/430 SypHer, F640/580 SNARF) were calculated in MetaFluor 6.3 (Universal Imaging) and analyzed in Excel (Microsoft) and GraphPad Prism 5.01 (GraphPad). After each experiment, cytosolic and mitochondrial pH was calibrated using nigericin (5 μg/ml) and monensin (5 μM) in 125 mM KCl, 20 mM NaCl, 0.5 mM $MgCl_2$, 0.2 mM EGTA, and 20 mM *N*-methyl-D-glutamine (pH 9.5–10.0), Tris (pH 8.0, 9.0), HEPES (pH 7.0–7.5), or MES (pH 5.5–6.5). For each cell, a 6-point calibration curve was fitted to a variable slope sigmoid equation with $1/y$ weighting and constraining the top of the curve to 30 (GraphPad Prism 5.01).

Ca^{2+} Imaging—Cytosolic Ca^{2+} was measured with fura-2 (2 μM) or YC3.6 (39), and mitochondrial Ca^{2+} with 4mitD3-CPV on the epifluorescence system described above. Fura-2 was excited alternately at 340 and 380 nm (200–300 ms/λ) through a 430DCLP dichroic filter and 510WB40 emission filter when recording only Fura-2 or through a 505DCXR dichroic filter and 535DF25 filter when measured simultaneously with SypHer. Cameleons were excited at 430 nm through a 455DRLP dichroic filter and alternately imaged with 475DF15 and 535DF25 emission filters (200–400 ms/λ, Omega Optical).

Cell Lysis, Mitochondrial Isolation, and Western Blotting—Whole cells were lysed in a glass homogenizer. The lysate was centrifuged at 14,000 × *g* for 20 min, and the protein content of the supernatant was determined using a BCA protein assay (Pierce). The mitochondrial fraction was obtained by differential centrifugation as reported previously (40). 20 μg of total protein (from cytosolic or mitochondrial fraction) was loaded per lane of SDS-PAGE. For immunoblotting, proteins were transferred onto nitrocellulose membrane and probed with the following antibodies: anti-GFP (sc-9996) and anti-Tom20 (sc-11415) (Santa Cruz Biotechnology, Inc. (Santa Cruz, CA) and anti-α-tubulin (T9026) (Sigma). Horseradish peroxidase-conjugated Secondary antibodies (Amersham Biosciences) were used, followed by detection by chemiluminescence (Amersham Biosciences).

Inmunocytochemistry and Confocal Imaging—48 h after transfection cells were fixed using 4% paraformaldhyde for 15 min, permeabilized with 0.1% Triton X-100 for 10 min, and incubated in blocking buffer IgG (2 μg/ml) for 1 h. Fixed cells were probed with rabbit polyclonal anti-Tom20 (1:100) for 10 h at 6 °C and labeled with Alexa Fluor 568-conjugated goat anti-rabbit IgG (1:1000) from Sigma for 1 h at room temperature. Confocal images were acquired on a Leica SP5 2 photon microscope using a ×63 oil immersion objective. MitoSypHer was excited at 488 nm, and fluorescence emitted between 510 and 540 nm was collected. Alexa Fluor 568 was excited at 561 nm, and fluorescence emitted between 600 and 630 nm was collected. The confocal pinhole was 154 μm (1 airy disk) for SypHer and 204 μm (1.25 airy disk) for Tom20.

Live Cell Confocal Imaging—Confocal images were acquired with a Zeiss LSM510meta, using a ×63 Achroplan water immersion objective (numerical aperture 0.95) and 12-bit acquisition mode with zoom set to give 130-nm pixels. For mitoSypHer/MitoTracker dual labeling, 2 days after mitoSypHer transfection, cells were incubated with 25 nM MitoTracker Red CMXRos for 45 min at 37 °C in normal culture medium. Medium was replaced with HBSS (ambient temperature) immediately before image acquisition. Images were acquired with simultaneous 488/561 nm excitation with sequential 490- and 565-nm dichroic filters and 505–550 nm bandpass emission (SypHer) and 575 nm longpass (MitoTracker Red CMXRos).

Calculation of H^+-buffering Power and Fluxes—Cytosolic and mitochondrial H^+-buffering powers (β) were calculated by measuring pH changes in cells exposed to permeant weak acid (butyric acid; $pK_a = 4.82$) or weak base (trimethylamine (TMA); $pK_a = 9.80$) and estimating the change in internal acid/base concentration as described previously (41). Some investigators assume that weak acids (bases) fully deprotonate (protonate) at physiological pH to simplify calculations. We found that this assumption systematically overestimated the calculated changes in weak acid and base, so we relied on exact calculation by the Henderson-Hasselbach equation. To ensure that we measured intrinsic cytosolic and matrix-buffering power, the Na^+/H^+ exchanger was inhibited with amiloride (100 μM), and the respiratory chain was inhibited with rotenone (5 μM), antimycin (5 μM), and oligomycin (5 μg/ml). The concentration of TMA in compartment j (cytosol or mitochondria) was estimated by Equation 1,

$$[TMAH^+]_j = \frac{[TMAH^+ + TMA]_k}{1 + 10^{(pK_a - pH_j)}} \times 10^{(pK_a - pH_j)} \qquad \text{(Eq. 1)}$$

where compartment k (extracellular space or cytosol) is the compartment immediately external to j, and pK_a^{TMA} is assumed to be equal in all compartments. For butyric acid, the same equation is used, but ($pH_j - pK_a$) replaces ($pK_a - pH_j$). Subsequently, β is calculated by Equation 2,

$$\beta_j = \Delta[TMAH^+]_j / \Delta pH_j \qquad \text{(Eq. 2)}$$

where $\Delta[TMAH^+]_j = [TMAH^+]_{j,final} - [TMAH^+]_{j,initial}$, calculated before and after a change in $[TMA]_{bath}$, and ΔpH_j is measured as the midpoint pH between changes in $[TMA]_{bath}$. Simultaneous measurements of pH_{cyto} and pH_{mito} permitted β_{mito} to be calculated from Equation 1, where the cytosol is compartment k.

High Throughput pH Imaging—Separate halves of a 96-well plate were transfected with SypHer and mitoSypHer. 48 h later, culture medium was replaced with HBSS, and the plate was placed in an ImageXpress Micro plate-reading microscope sys-

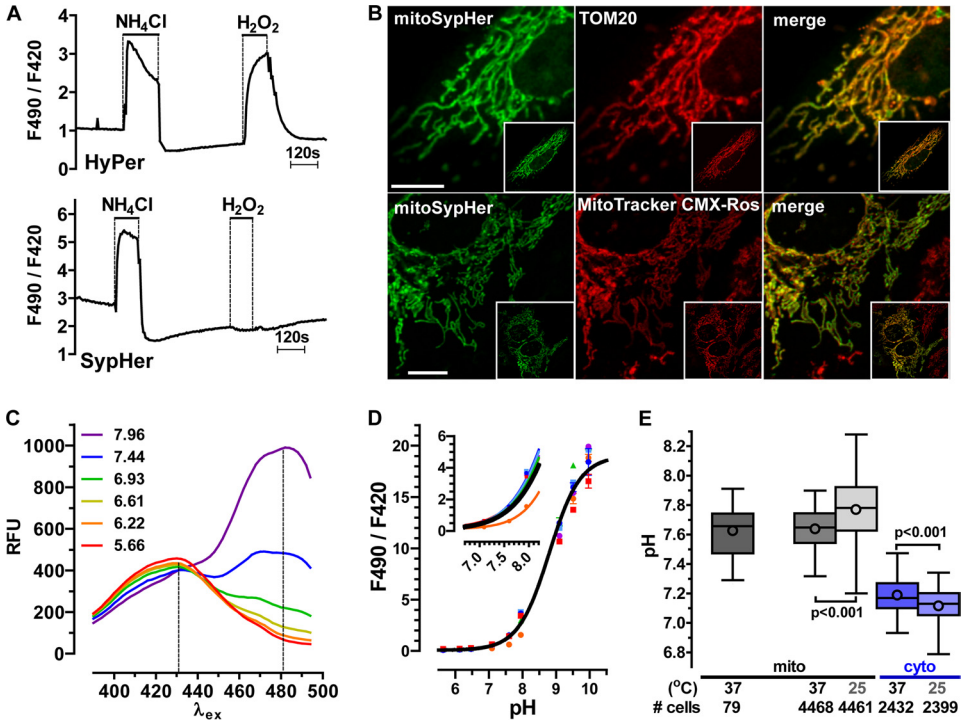

FIGURE 1. **SypHer characterization.** *A*, changes in HyPer (*top*) and SypHer ratio (*bottom*) evoked by an alkaline load (30 mM NH_4Cl) and by H_2O_2 (200 μM). *B*, confocal images of mitoSypHer (*green*) in fixed cells stained for TOM20 (*red*; *top*) or live cells labeled with MitoTracker Red CMXRos (*red*; *bottom*). *Merged images* (*right*) show clear mitochondrial targeting of mitoSypHer. *Scale bars*, 5 μm (*top*) and 10 μm (*bottom*). *C*, excitation spectra of mitoSypHer *in situ*, at 37 °C using a 505-nm dichroic and 535/25 emission filter. *D*, *in situ* calibration of mitoSypHer. *Inset*, dynamic range at physiological pH. *E*, average resting pH_{cyto} and pH_{mito} measured by single-cell (*left box*) and high throughput fluorescence imaging. *Boxes* show quartiles with *circles* centered on means; *error bars* show S.E. for the individual cells and 95% intervals for high throughput data.

tem (Universal Imaging, Sunnyvale, CA) (humidified, 37 °C). Using laser-assisted autofocusing and automated image acquisition (20× objective, 0.5 numerical aperture), ratio images (F480: ex_1 470/45 nm, 500 $dichroic_1$, em_1 520/40; F430: ex_2 435/25 nm, 465 nm $dichroic_2$, em_2 480/35 nm) were acquired over the same grid pattern in each well (4–12 sites/well) with a 12-bit CCD camera. For histamine stimulations, 100 μl of 2× concentrated histamine was added to 100 μl of HBSS in each well with a multichannel pipette, and recording was started within 1 min of the addition. On each plate, SypHer and mitoSypHer ratios were calibrated such that intracellular pH for one well for each probe was clamped at 5.5, 6.0, 6.5, 7.0, 7.5, and 8.0 (supplemental Fig. S3*A*). We created automated algorithms (MetaXpress, Universal Imaging) to define regions around cells in F480 images, to calculate background fluorescence and subtract it from the average F80 and F430 fluorescence intensity in each defined cell region. Single-cell fluorescence values (50–400 per well) were transferred to Excel for sorting and calibration of ratio values. For each well, cells with ratio values greater than two S.D. from the mean value were excluded, and individual ratio values were calibrated against a standard curve generated on each plate.

RESULTS

Probe Generation and Validation—While testing the properties of HyPer, a commercial H_2O_2-sensing probe based on a circularly permuted YFP (38), we observed that HyPer exhibited ratiometric responses to NH_4^+-induced (30 mM) matrix alkalinization of similar amplitude to its responses to H_2O_2 (200 μM) (Fig. 1*A*, *top*). We reasoned that HyPer could provide the basis for a ratiometric pH sensor with excellent mitochondrial targeting and brightness. We generated a pH-specific version of HyPer that we dubbed SypHer (synthetic pH sensor) by mutating one of the two H_2O_2-sensing cysteine residues (C199S) of HyPer, as described by Belousov *et al.* (38). As expected, cells expressing cytosolic SypHer still exhibited large fluorescence changes upon the addition of NH_4^+ but failed to respond to H_2O_2 (Fig 1*A*, *bottom*). We then characterized the properties of the SypHer probe *in vitro*, using protein extracts from HeLa cells expressing cytosolic SypHer. As shown in supplemental Fig. S1, the fluorescence intensity increased markedly with pH at excitation wavelength exceeding 435 nm, with a peak around 490 nm. The 490/420 fluorescence ratio was not altered by the addition of millimolar concentrations of Ca^{2+}, PO^{4-}, and H_2O_2 (Table 1) but increased by ~5-fold when the bath pH was increased from 7.0 to 8.0 (supplemental Fig. S1*B*).

TABLE 1

***In vitro* characterization of SypHer sensitivity to various ions and oxidizing and reducing agents**

Cell lysates from SypHer-expressing cells were prepared in 100 mM HEPES, 150 mM NaCl, 0.5 mM β-mercaptoethanol, pH 7.00 (n = 3) and 7.45 (n = 3).

Compound	Concentration	Change in ratio (490/440) at pH 7.00	Change in ratio (490/440) at pH 7.45
	mM	*-fold*	*-fold*
NaOH (pH 7.00–7.76)	40	2.19 ± 0	
NO (SNAP)	0.1	0.99 ± 0.005	1.00 ± 0.002
DTT	1.0	0.99 ± 0.004	1.00 ± 0.004
H_2O_2	0.1	1.00 ± 0.004	0.99 ± 0.001
Ca^{2+}	1.0	1.01 ± 0.006	1.00 ± 0.006
PO_4^-	1.0	1.01 ± 0.009	1.00 ± 0.004

MitoSypHer was efficiently targeted to the mitochondrial matrix by tandem mitochondrial localization sequences, as demonstrated by its colocalization with the mitochondrial resident protein TOM20 and with MitoTracker (Fig. 1*B*, Pearson coefficients 0.88 ± 0.03 and 0.91 ± 0.06, $n = 4$ and 5 cells, respectively) and enriched reactivity for an anti-GFP antibody in mitochondrial fractions (supplemental Fig. S2*A*). Mitochondria-targeted SypHer (mitoSypHer) had spectral properties similar to its parental probe (Fig. 1*C*) and displayed opposite changes in fluorescence at $\lambda_{ex} = 420$ and $\lambda_{ex} = 490$ when the pH of the organelle was varied with H^+ ionophores (supplemental Fig. S2*B*). Using an automated microscope to image cells on 96-well plates, equilibration of the extracellular and organellar pH with H^+ ionophores confirmed that the mitoSypHer ratio reported variations in local pH and that resting pH_{mito} in most cells was between 7.5 and 8.0 (supplemental Fig. S3*A*). pH titration curves generated from different wells of the 96-well plate clamped at specific pH values and with cells expressing cytosolic or mitochondria-targeted SypHer closely overlapped (supplemental Fig. S3*B*), demonstrating that the pH responses of SypHer were not altered by the matrix environment and that the calibration protocol equilibrated both compartments. *In situ* calibration of mitoSypHer ratio against pH showed a pK_a of 8.71 ± 0.05 and a Hill slope of 0.96 ± 0.05 (Fig. 1*D*) with an impressive 20-fold increase in ratio when pH increased from 7 to 10. The ratio increased 4-fold in the more physiological pH range of 7–8, (Fig. 1*D*, *inset*), permitting accurate measurements of pH_{mito}. Having validated the probe, we next measured resting pH_{mito} on the standard epifluorescence microscope, generating an autonomous calibration curve for each cell imaged. To our surprise, resting pH_{mito} (7.61 ± 0.02, minimum 7.26, maximum 7.91, 79 cells; Fig. 1*E*) was notably lower than the values of 7.8–8.1 previously reported in intact cells (42–44). To confirm these observations, we measured pH_{mito} and pH_{cyto} with SypHer in a large number of cells, by imaging 96-well plates (supplemental Fig. S3). Mitochondrial pH was 7.64 ± 0.14 (mean ± S.D.) at 37 °C and significantly higher (7.77 ± 0.26, mean ± S.D.) at 25 °C (Fig. 1*E*), consistent with reports that isolated mitochondria are more polarized at 28 °C *versus* 37 °C (45). In contrast, pH_{cyto} was slightly higher at 37 °C (7.19 ± 0.14) than at 25 °C (7.12 ± 0.14). Consequently, the pH gradient across the inner mitochondrial membrane, ΔpH_m, averaged 0.46 units in resting, non-stimulated HeLa cells at 37 °C and increased to 0.65 units when the temperature was decreased to 25 °C. The resting pH_{mito} and ΔpH_m of quiescent cells at physiological temperatures were thus lower than previously reported.

Mitochondrial pH Decreases during Cytosolic Ca^{2+} Elevations—Cytosolic Ca^{2+} elevations boost mitochondrial metabolism, but whether this effect involves net changes in pH_{mito} is controversial because both alkalinization and acidification of mitochondria have been reported during $[Ca^{2+}]_{cyt}$ elevations (42, 43, 46–48). To determine how changes in $[Ca^{2+}]_{cyt}$ alter ΔpH_m, HeLa cells expressing mitoSypHer were loaded with the Ca^{2+}-sensitive dye fura-2 to monitor $[Ca^{2+}]_{cyt}$ and pH_{mito} simultaneously. The $[Ca^{2+}]_{cyt}$ elevations evoked by the Ca^{2+}-mobilizing agonist histamine were associated with a significant decrease in pH_{mito} (Fig. 2*A*), but the $[Ca^{2+}]_{cyt}$ and

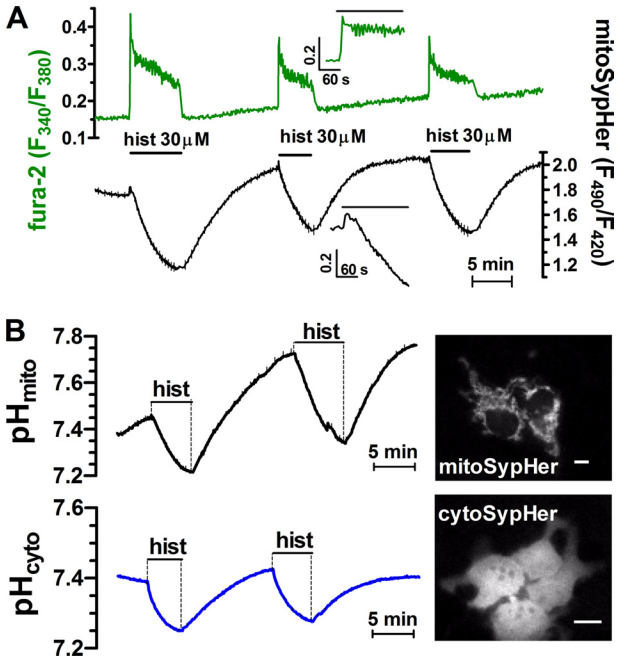

FIGURE 2. **Mitochondria acidify during $[Ca^{2+}]_{cyt}$ elevations.** *A*, $[Ca^{2+}]_{cyt}$ responses to histamine measured with fura-2 (*green*; raw ratio) in cells expressing mitoSypHer (*black*; raw ratio). *Traces* show the mean response of seven cells in a single field of view with an *inset* of simultaneous responses from a single cell. *B*, parallel pH_{mito} (*black*, mitoSypHer; mean of 11 cells) and pH_{cyto} (*blue*, cytoSypHer; mean of four cells) acidification following a 30 μM histamine addition. *Scale bars*, 10 μM.

pH_{mito} responses had different temporal profiles. The $[Ca^{2+}]_{cyt}$ elevation exhibited a transient peak followed by a sustained plateau, whereas the pH_{mito} decay was monophasic (Fig. 2*A*), even in cells that exhibited Ca^{2+} oscillations during the sustained phase of the Ca^{2+} signal (Fig. 2*A*, *insets*). Parallel pH_{cyto} recordings with cytosolic SypHer revealed parallel decreases in pH_{cyto} during $[Ca^{2+}]_{cyt}$ elevations but with a smaller amplitude than decreases of pH_{mito} (Fig. 2*B*). Interestingly, the larger decrease in pH_{mito} than pH_{cyto} was more pronounced during the second histamine stimulation (Fig. 2*B*). Cell-to-cell variability limited our ability to measure precisely ΔpH_m in individual cells from independent recordings of pH_{cyto} and pH_{mito}. To overcome this limitation, we simultaneously measured pH_{mito} using mitoSypHer and pH_{cyto} using the pH indicator SNARF, a red-shifted dye whose fluorescence emission does not overlap with the yellow fluorescence of mitoSypHer (Fig. 3*B*). Calculating the cellwise difference between the pH_{mito} and pH_{cyto} recordings (*black* and *blue traces*, respectively), these concurrent measurements enabled us to follow ΔpH_m (*red trace* in the *bottom panel*) in intact cells. As shown in Fig. 3*A*, each histamine stimulation decreased ΔpH_m by ~0.05 (range 0.06 to −0.28; Fig. 3*C*, *iii*) because drops in pH_{mito} typically exceeded those in the cytosol. Upon histamine removal, pH_{cyto} recovered to resting levels, whereas a pH_{mito} overshoot was typical following successive stimulations (Fig. 3*A*). As a result, ΔpH_m increased from 0.15 ± 0.02 in "resting" cells to 0.44 ± 0.02 following recovery from a third histamine stimulation (Fig. 3*C*, *iv*). Using the high throughput imaging, we also observed that histamine-mediated acidification was concentration-dependent and maintained during 25–30 min of stimulation with only modest recovery (supplemental Fig. S3*D*).

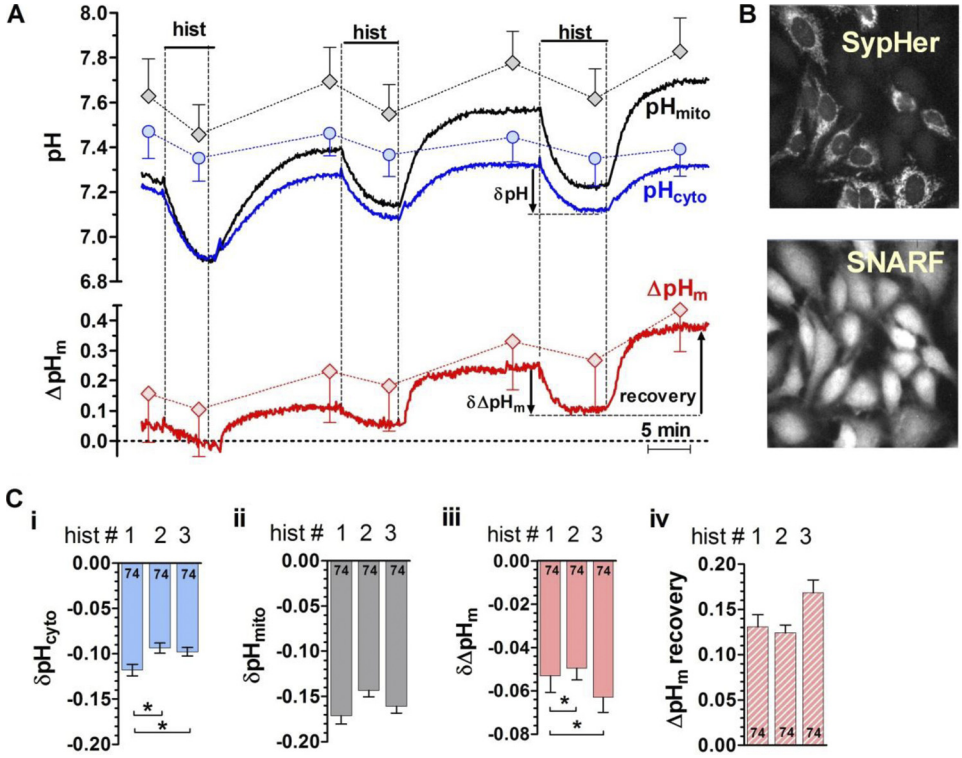

FIGURE 3. **ΔpH_m changes during and after $[Ca^{2+}]_{cyt}$ elevations.** *A*, simultaneous pH_{mito} (*black*, mitoSypHer) and pH_{cyto} (*blue*, SNARF) measurements in cells repeatedly stimulated with histamine (30 μM). For each cell, ΔpH_m was estimated as $pH_{mito} - pH_{cyto}$ (*red*). *Diamonds* and *circles*, mean ± S.D. from 74 cells. *B*, typical mitoSypHer (*top*, λ_{ex} 480 nm) and SNARF fluorescence images (*bottom*, λ_{em} 580 nm). *C*, average changes in pH_{cyto} (*i*), pH_{mito} (*ii*), and ΔpH_m (*iii*) during each histamine addition and in ΔpH_m (*iv*) after histamine washout (mean ± S.E. (*error bars*) of 74 cells). *, $p < 0.05$ for repeated measures general linear model analysis of variance.

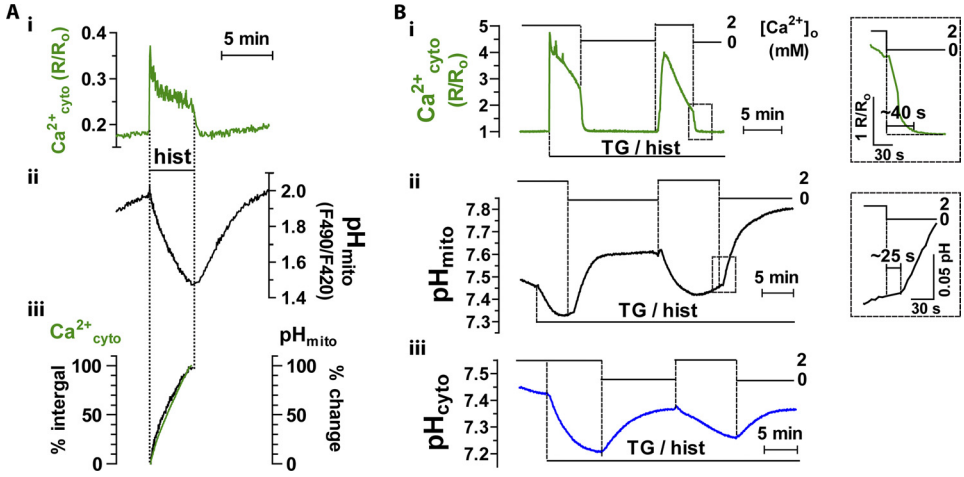

FIGURE 4. **Ca^{2+} dependence of the decreases in mitochondrial and cytosolic pH.** *A*, simultaneous $[Ca^{2+}]_{cyto}$ (*i*; fura) and pH_{mito} (*ii*; mitoSypHer) recordings illustrate that the change in mitoSypHer ratio (*iii*; *black*) closely match the instantaneous integral of the fura-2 ratio (*iii*; *green*). Traces are taken from Fig. 2*A*. *B*, effect of extracellular Ca^{2+} removal and restitution on $[Ca^{2+}]_{cyt}$ (YC3.6 cameleon, 4 cells) (*i*), pH_{mito} (11 cells) (*ii*), and pH_{cyto} (nine cells) (*iii*) responses evoked by histamine (30 μM) and thapsigargin (1 μM). *Insets* show kinetics of SERCA-independent Ca^{2+}_{cyto} clearance (*i*) and pH_{mito} recovery (*ii*).

$[Ca^{2+}]_{cyt}$ Dependence of the Decreases in pH_{mito} and pH_{cyto}—A close inspection of Ca^{2+} and pH responses evoked by histamine revealed that the kinetics of acidification closely matched the instantaneous integral of the Ca^{2+} elevation, suggesting that acid accumulation was proportional to the total cytosolic Ca^{2+} load rather than its instantaneous concentration (Fig. 4*A*). The typical peak-and-plateau $[Ca^{2+}]_{cyt}$ response to histamine is due to initial Ca^{2+} release from the endoplasmic reticulum through inositol 1,4,5-trisphosphate receptors, followed by sustained Ca^{2+} influx across store-operated Ca^{2+} entry channels. To determine if $[Ca^{2+}]_{cyt}$ was necessary for the intracellular acidification, we treated cells with 2-APB, an inhibitor of both inositol 1,4,5-trisphosphate receptor intracellular Ca^{2+} release channels and store-operated Ca^{2+} channels. As expected, 2-APB (75 μM) inhibited both the release and influx components of $[Ca^{2+}]_{cyt}$ elevations measured with the FRET-based YC3.6, reducing the integrated Ca^{2+} response by 86.2 ± 1.7% (supplemental Fig. S4, *A* and *C*). In parallel, 2-APB impaired pH_{cyto} and pH_{mito} decreases and completely prevented the loss of ΔpH_m evoked by histamine

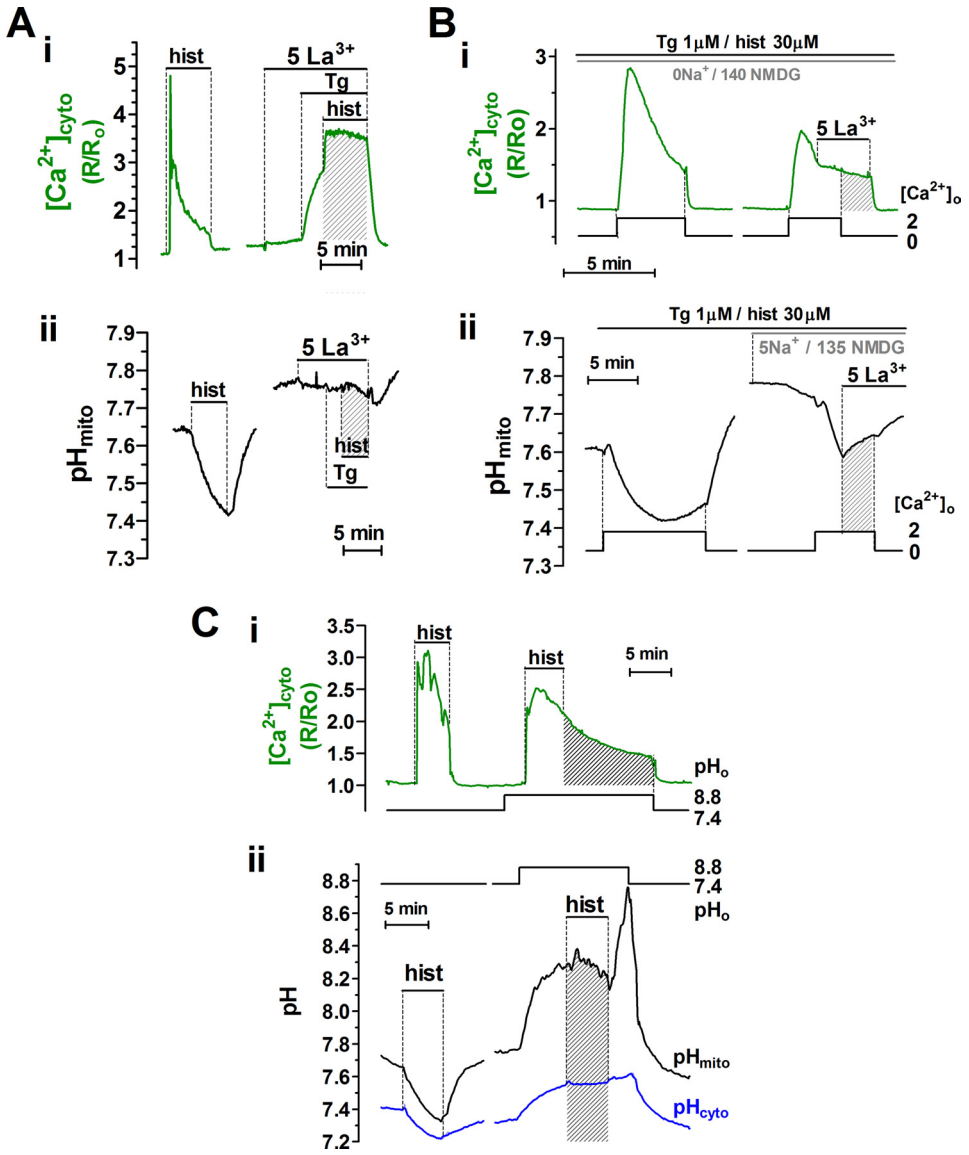

FIGURE 5. **PMCA mediates the Ca^{2+}-dependent decreases in pH_{cyto} and pH_{mito}.** *A*, La^{3+} (5 mM) blocks clearance of a $[Ca^{2+}]_{cyt}$ elevation (*i*) and decrease in pH_{mito} (*ii*) evoked by histamine (30 μM) when SERCA is blocked with thapsigargin (*Tg*; 1 μM). *B*, effect of La^{3+} (5 mM) on the clearance of $[Ca^{2+}]_{cyt}$ elevations (*i*) and on decreases in pH_{mito} (*ii*) evoked by Ca^{2+} readdition to cells treated with histamine and thapsigargin in low extracellular Na^+ to block Ca^{2+} clearance by the Na^+/Ca^{2+}-exchanger. *C*, effect of alkaline pH_o (8.8) on $[Ca^{2+}]_{cyt}$ (YC3.6 cameleon, four cells) recovery (*i*) after histamine removal and the decrease in pH_{cyto} (SNARF) and pH_{mito} (mitoSypHer) (*ii*) evoked by histamine. La^{3+} and alkaline pH_o both prevent Ca^{2+} clearance and prevent the decreases in cytosolic and mitochondrial pH.

(supplemental Fig. S4, *B*, *D*, and *E*). To separate the influx from the release component of the $[Ca^{2+}]_{cyt}$ elevation, cells were treated with histamine in the presence of thapsigargin (1 μM) to inhibit the sarco/endoplasmic reticulum Ca^{2+} ATPase (SERCA) and to deplete endoplasmic reticulum Ca^{2+} stores. Subsequent restitutions of external Ca^{2+} caused large $[Ca^{2+}]_{cyt}$ elevations due to Ca^{2+} entry through store-operated Ca^{2+} entry channels that were sufficient to induce massive decreases in pH_{cyto} and pH_{mito} (Fig. 4*B*, *i* and *ii*). Rapid Ca^{2+} extrusion was initiated immediately upon removal of extracellular Ca^{2+}, whereas the onset of pH recovery was delayed until $[Ca^{2+}]_{cyt}$ was almost at resting levels (Fig. 4C, *i* and *ii*, *insets*). Thus, Ca^{2+}-dependent acidification did not require the activity of SERCA, and all conditions that caused $[Ca^{2+}]_{cyt}$ elevations decreased both pH_{cyto} and pH_{mito}.

PMCA Underlies the Ca^{2+}-dependent Decreases in pH—Like SERCA, PMCA catalyzes H^+/Ca^{2+} countertransport (49, 50) (reviewed in Refs. 51 and 52). Several lines of evidence indicate that the activity of the PMCA could account for the drop in pH associated with $[Ca^{2+}]_{cyt}$ elevations. First, La^{3+}, at millimolar concentrations known to inhibit the PMCA (53), completely inhibited histamine-induced decreases in pH_{cyto} (not shown) and pH_{mito} while enhancing $[Ca^{2+}]_{cyt}$ elevations (Fig. 5*A*). Because La^{3+} is not a specific inhibitor of PMCA, we attempted to isolate the activity of the PMCA by treating cells with thapsigargin and reducing extracellular Na^+ to 0–5 mM to inhibit the NCX. Under these conditions, the activity of the PMCA is directly reflected by the rapid decrease in $[Ca^{2+}]_{cyt}$ upon the removal of extracellular Ca^{2+}. As expected, La^{3+} (5 mM) rapidly and reversibly blocked this $[Ca^{2+}]_{cyt}$ recovery (Fig. 5*B*, *i*), with

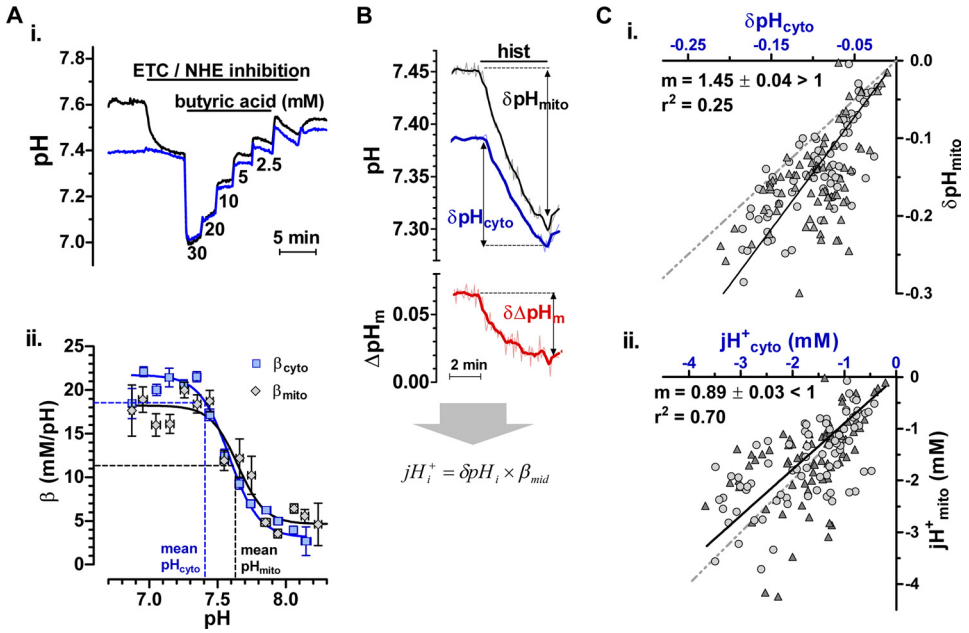

FIGURE 6. **Low mitochondrial buffering power at alkaline pH_{mito} underlies the loss of ΔpH_m during Ca^{2+} elevations.** *A*, *i*, protocol used to calculate H^+-buffering power (β) by the stepwise addition/removal of permeant weak acid. *Black traces*, mitoSypHer; *blue traces*, SNARF. Amiloride (100 μM), rotenone (5 μM), antimycin (5 μM), and oligomycin (5 μg/ml) were added to prevent membrane H^+ transport. *ii*, pH dependence of intrinsic H^+-buffering power (β_{cyto} and β_{mito}). β values were binned every 0.1 pH units (mean ± S.E.). *Dotted lines*, β at mean resting pH_{cyto} and pH_{mito}. *Solid lines*, fitted sigmoid functions. *B*, calculation of J_{H^+} for a given histamine-mediated pH change, where β is a function of pH. *C*, *i*, changes in pH_{mito} as a function of the changes in pH_{cyto} in the same cell during histamine responses. Regression of δpH_{mito} against δpH_{cyto} has a slope of >1, reflecting the loss of ΔpH_m during stimulation. *ii*, mitochondrial *versus* cytosolic proton fluxes. Regression of the calculated J_{H^+mito} *versus* J_{H^+cyto} has a slope of <1, indicating that mitochondria resist cytosolic H^+ fluxes. Regressions were constrained to pass through the origin.

an apparent IC_{50} of 0.2–0.3 mM (data not shown). Importantly, La^{3+} not only completely blocked the pH_{cyto} decrease initiated by $[Ca^{2+}]_{cyt}$ elevation (not shown), but it revealed a Ca^{2+}-dependent pH_{mito} alkalinization, particularly under conditions of low extracellular Na^+ (Fig. 5*B*, *ii*). The PMCA is also inhibited at alkaline extracellular pH (pH_o) because the ATPase is starved for protons to exchange with cytosolic Ca^{2+} (54). Increasing pH_o to 8.2–8.8 prevented the rapid recovery of $[Ca^{2+}]_{cyt}$ upon the removal of histamine, whereas subsequent restoration of physiological pH_o (7.4) caused an immediate decrease in $[Ca^{2+}]_{cyt}$, demonstrating the inhibition of the PMCA at alkaline pH_o (Fig. 5*C*, *i*). In parallel experiments, alkaline pH_o prevented the histamine-induced drop in pH_{cyto} and pH_{mito} (Fig. 5*C*, *ii*), consistent with a role for the PMCA in the acid generation. Inhibition of PMCA has also been shown for orthovanadate, with sensitivities ranging from micromolar to millimolar concentrations (53). We observed little to no inhibition of histamine-induced acidification at micromolar concentrations of orthovanadate, but 1 and 10 mM orthovanadate inhibited both pH_{cyto} and pH_{mito} acidifications by ~30% (data not shown). Thus, regardless of the approach used to inhibit PMCA, decreased Ca^{2+} extrusion was consistently associated with decreased cellular acidification, strongly suggesting that PMCA was the main source of the acid generated during $[Ca^{2+}]_{cyt}$ elevations.

Influence of Mitochondrial H^+-buffering Power on ΔpH_m—Mitochondria consistently showed larger decreases in pH than concomitant changes in the cytosol during histamine stimulations. The larger pH_{mito} decrease caused a net loss of ΔpH_m during each agonist application (Fig. 3), to the extent that the loss of ΔpH_m showed a linear correlation with the absolute value of pH_{mito} immediately prior to the histamine addition (not shown). The net loss of ΔpH_m during histamine-mediated pH_{cyto} acidification could reflect the facilitated import of protons across the inner mitochondrial membrane. Alternatively, the different amplitudes of decreases in pH_{mito} and pH_{cyto} might reflect different proton buffering capacities (β) of the cytosol and mitochondria. High concentrations of cytosolic pH buffers mitigate intracellular pH changes during surges of intracellular acid production. A lesser pH buffering capacity of mitochondria compared with the cytosol might therefore cause a greater decrease in pH_{mito} than pH_{cyto} for an identical acid load. The pH buffering capacity of the cytosol (β_{cyto}) is reported to be 20–30 mM (55), but the intrinsic buffering power of mitochondria (β_{mito}) has not been determined to date. To obtain this parameter, we simultaneously measured the pH_{mito} and pH_{cyto} changes evoked by the addition of varying concentrations of permeant weak acids (butyric acid) or bases (trimethylamine), the former illustrated in Fig. 6*A*, *i*. This well established procedure (41) enabled us to determine the buffering power of the cytosol and of mitochondria, over the physiological range of pH 6.8–8.4. As shown in Fig. 6*A*, *ii*, the pH dependence of β_{cyto} and β_{mito} was similar (pK_{acyto} 7.58 ± 0.01, pK_{amito} 7.65 ± 0.03), suggesting that the nature of the pH buffers is similar in both compartments. Reassuringly, measurements of β_{cyto} (20.7 ± 1.3 mM) at physiological pH_{cyto} (6.9–7.4) were consistent with previous reports (55). Over the same pH range, β_{mito} was measurably lower (17.8 ± 1.6 mM, $p = 0.012$, general linear model analysis of variance). More importantly, both β_{cyto} and β_{mito} rapidly fell at pH values above ~7.4, such that β_{mito} (~10 mM) was roughly half of β_{cyto} at the typical resting pH_{mito} of ~7.6. These experiments provide the first estimates of the

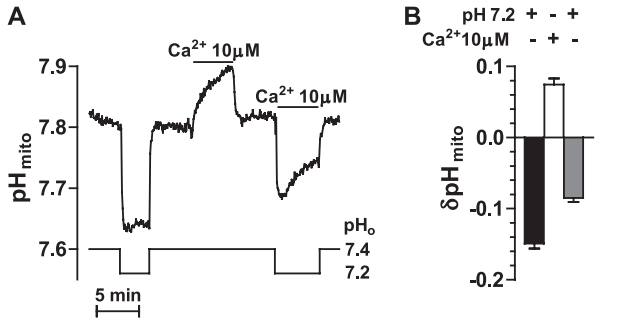

FIGURE 7. **Opposite effects of Ca^{2+} and H^+ on mitochondrial matrix pH.** *A*, pH_{mito} responses evoked by the addition of H^+ and Ca^{2+} to permeabilized cells. Bath pH was transiently decreased from 7.4 to 7.2, and then 10 μM Ca^{2+} was added at pH 7.4 or during the pH switch to mimic the changes occurring in intact cells. *B*, averaged pH_{mito} responses evoked in permeabilized cells by a decrease in environmental pH to 7.2, by the addition of 10 μM Ca^{2+} at pH 7.4, or by the addition of 10 μM Ca^{2+} during a switch to pH 7.2.

pH dependence of β_{mito} and indicate that the buffering capacity of mitochondria rapidly decreases as the organelle alkalinizes. This strongly suggests that the reduced H^+ buffering capacity of mitochondria at alkaline pH underlies the loss of ΔpH_m during histamine stimulation.

To quantify the effect of the differential buffering capacity of the two compartments, we used the measured β_{cyto} and β_{mit} values to calculate the net fluxes of protons (J_{H^+}) underlying the typical pH_{cyto} and pH_{mito} responses in a random subset of cells (Fig. 6*B*). As expected, correlation of the amplitude of the drop in pH_{mito} (δpH_{mito}) with the drop in pH_{cyto} (δpH_{cyto}) produced a regression slope greater than 1, consistent with the loss of ΔpH_m (Fig. 6*C*, *i*). When changes in pH were converted to net H^+ fluxes (J_{H^+}) with the formula, $J_{H^+i} = \delta pH_i \times \beta_i$, the positive correlation was retained but with a slope significantly less than unity (Fig. 6*C*, *ii*). This meant that the flux of protons reaching the matrix was smaller than the flux of protons entering the cytosol, as expected given that the inner mitochondrial membrane is not freely permeable to protons. Thus, the loss of ΔpH_m was probably due to the difference between β_{mito} and β_{cyto} at physiological pH values in each compartment. Combined, these findings show that the absolute value of pH_{mito} prior to a stimulus like histamine and the pH dependence of β_{mito} are important, previously unrecognized determinants of the changes in pH_{mito} and ΔpH_m occurring in living cells.

Ca^{2+} and H^+ Have Opposite Effects on Mitochondrial Matrix pH—The drop in pH_{mito} observed during $[Ca^{2+}]_{cyt}$ elevations is at odds with the known effect of mitochondrial Ca^{2+} uptake to cause matrix alkalinization (17). To study whether the decrease in mitochondrial pH was due to the concomitant cytosolic acidification that occurred during the $[Ca^{2+}]_{cyt}$ elevation, we measured the changes in pH_{mito} in permeabilized cells exposed to Ca^{2+} or pH changes. As shown in Fig. 7, a transient decrease in bath pH from 7.4 to 7.2 rapidly and reversibly decreased the matrix pH by ~0.15 pH units. The subsequent addition of 10 μM Ca^{2+} at pH 7.4 evoked a matrix alkalinization that developed more slowly and that was of smaller amplitude, increasing matrix pH by ~0.08 pH unit. Parallel experiments in cells expressing 4mitD3-CPV revealed that the addition of Ca^{2+} to permeabilized cells caused robust $[Ca^{2+}]_{mit}$ elevations that were largely prevented by inhibition of the Ca^{2+} uniporter with Ru360 (supplemental Fig. S5*A*). We then added 10 μM Ca^{2+} during the switch to pH 7.2 to mimic the Ca^{2+} and pH changes occurring in intact cells stimulated with histamine. This protocol caused a rapid decrease in pH_{mito} followed by a slow recovery to a steady-state value ~0.09 pH units more acidic than the initial pH_{mito} (Fig. 7). Thus, mitochondria showed the expected pH_{mito} increase in response to Ca^{2+} elevations, but this alkalinization was masked by a larger acidification when pH_{cyto} was decreased concomitantly.

Contributions of Mitochondrial Transporters to Mitochondrial H^+ Fluxes—The large flux of protons reaching the mitochondrial matrix when the cytosol acidifies indicates that pH_{cyto} and pH_{mito} are in dynamic equilibrium. This is not surprising, given the multiplicity of H^+-coupled transporters present in the inner mitochondrial membrane, and we then attempted to identify pharmacologically the transporters involved. Cells were stimulated repeatedly with histamine as in Fig. 3, and inhibitors were added 5 min before the third stimulation. We first inhibited the electron transport chain (ETC) with rotenone and antimycin to block complexes I and III, respectively. As expected, inhibition of the ETC caused an immediate decrease in pH_{mito} and collapsed ΔpH_m to 30% of resting levels. In these conditions, the decrease in pH_{mito} evoked by histamine closely matched that of pH_{cyto}, and the histamine-induced loss of ΔpH_m was precluded (Fig. 8*A*). To quantify the effect of ETC inhibition on mitochondrial H^+ fluxes, the ratio of net J_{H^+mito} to net J_{H^+cyto} evoked by histamine was compared in single cells before and after the addition of inhibitors (or vehicle) to account for cell to cell variability in J_{H^+cyto}. As shown in Fig. 8*C*, ETC inhibition reduced J_{H^+mito}/J_{H^+cyto} by ~28 ± 18%. We then used oligomycin to inhibit the F_1F_0-ATP synthase. Contrary to our expectations, the addition of oligomycin did not increase pH_{mito} over a 5-min period in a majority of cells, possibly because mitochondria were already maximally alkaline after two successive stimulations with histamine. Oligomycin had no apparent effect on the subsequent decrease in pH_{cyto}, pH_{mito}, and ΔpH_m evoked by a third addition of histamine, and calculation of the protons fluxes revealed that oligomycin did not significantly reduced the average J_{H^+mito}/J_{H^+cyto} (Fig. 8*C*). Bongkrekic acid, an inhibitor of the adenine nucleotide transloctor, rapidly and selectively acidified mitochondria but did not significantly alter the J_{H^+mito}/J_{H^+cyto} (Fig. 8*C*). Thus, only inhibition of the ETC consistently decreased proton fluxes (by 20–25%), but this inhibition was associated with a decreased proton-motive force. Next, we investigated whether the mitochondrial Na^+/Ca^{2+} exchanger (NCLX), the major mitochondrial Ca^{2+} extruder of HeLa cells (56), participates in the rapid flux of protons into the matrix during cytosolic Ca^{2+} elevations. NCLX activity requires a mitochondrial Na^+ gradient generated and maintained by the mNHE, thus effectively coupling the extrusion of one Ca^{2+} ion with the entry of three protons into the mitochondrial matrix (7). To examine the contribution of the mNCX/mNHE axis to net mitochondrial H^+ flux, we used CGP-37157 to inhibit the NCLX (Fig. 8*A*). CGP-37157 reduced and delayed the onset of pH_{cyto} and pH_{mito} acidification, consistent with Ca^{2+} sequestration in mitochondria and reduced PMCA activity. Importantly, CGP-37157 reduced J_{H^+mito}/J_{H^+cyto} by ~45%

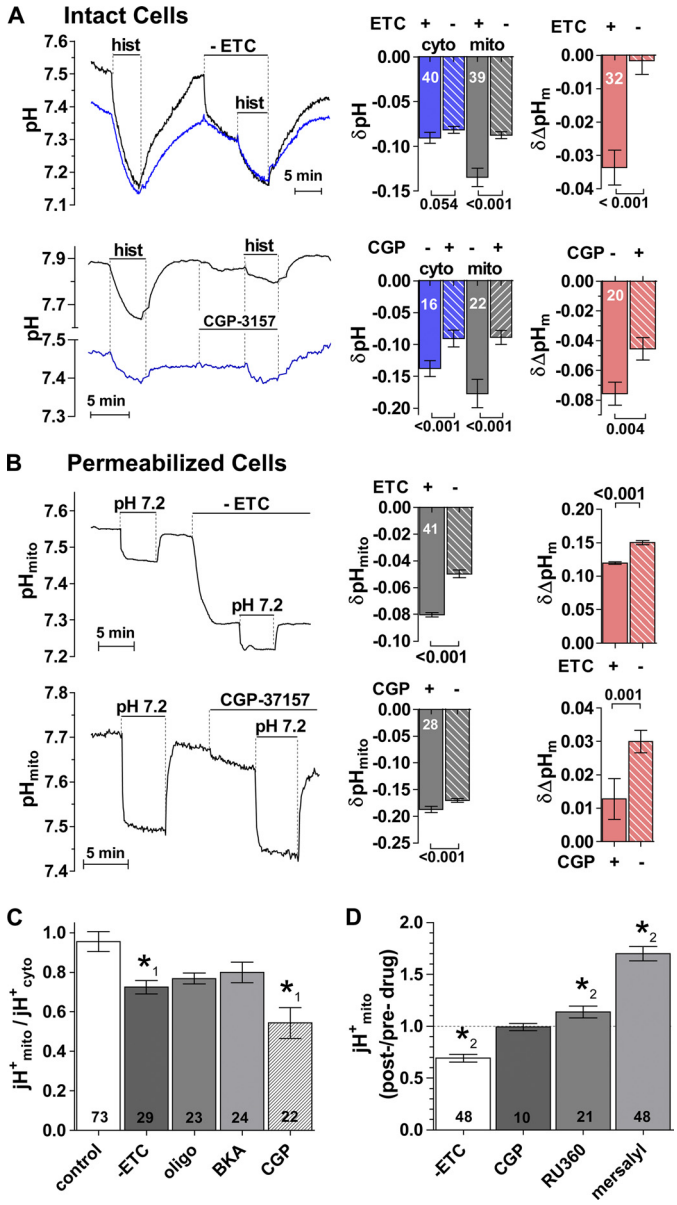

FIGURE 8. **Contributions of mitochondrial transporters to mitochondrial proton fluxes.** *A*, effects of inhibitors of the ETC (5 μM rotenone, 5 μM antimycin with or without 5 μg/ml oligomycin) and of the mitochondrial NCX (10 μM CGP-37157) on histamine-mediated pH_{mito} (*black*, mitoSypHer) and pH_{cyto} (*blue*, SNARF) responses in intact cells. *Bar graphs* show mean ± S.E. drug effects for pH_{cyto} (*blue*) and pH_{mito} (*gray*) acidification and loss of ΔpH_m (*pink*). *n* is displayed in the *bars* and *p* values are shown for *t* tests. *B*, effects of inhibitors of the ETC and of the mitochondrial NCX (as above) on the pH_{mito} responses evoked by the addition of H^+ to permeabilized cells. Bath pH was transiently decreased from 7.4 to 7.2 before and after the addition of the inhibitors. *Bar graphs* show mean ± S.E. decrease in pH_{mito} evoked by the pH switch from 7.4 to 7.2. *C*, average effect of the inhibitors on the J_{H^+mito}/J_{H^+cyto} flux ratio measured in intact cells during the third histamine response, using the second histamine response as internal control. *Bars*, mean ± S.E. (*error bars*) from *n* cells (*number* in *bars*) from ≥6 coverslips. $*_1$, significantly different from control by Dunnett's test with groupwise $\alpha = 0.05$. *D*, average effect of the inhibitors on the J_{H^+mito} flux measured in permeabilized cells during a pH switch from 7.4 to 7.2. $*_2$, significantly different ($p < 0.05$) by one-sample *t* test from internal control in the absence of inhibitor.

(Fig. 8*C*), suggesting that the mNCX/mNHE axis is implicated in the rapid transmission of protons from the cytosol to the mitochondrial matrix.

Because our pharmacological analysis of intact cells did not reveal a single clear mechanism of rapid proton flux across the mitochondrial membrane, we turned to permeabilized cells to clarify the mechanisms contributing to the high permeability of mitochondria for protons. As shown in Fig. 8*B*, the combination of oligomycin, antimycin, and rotenone rapidly decreased pH_{mito}, consistent with inhibition of the ETC. Under these conditions, the amplitude of the drop in pH_{mito} evoked by a rapid drop in bath pH was reduced by ~38%, and the calculated proton flux was reduced by 30% (Fig. 8*D*). In contrast, resting pH_{mito} as well as acid-induced proton fluxes were not affected by Ru360 and CGP 37157 (Fig. 8, *B* and *D*). Consistent with inhibition of mitochondrial Ca^{2+} uptake and extrusion, Ru360 reduced the pH_{mito} elevations evoked by the addition of Ca^{2+} to permeabilized cells (supplemental Fig. S5*B*), whereas CGP 37157 potentiated the Ca^{2+}-induced matrix alkalinization (supplemental Fig. S5*C*). Finally, we tested the effects of the P_i/H^+ symport inhibitor mersalyl. Mersalyl (100 μM) induced a rapid increase in matrix pH, followed by a subsequent decrease that was associated with a 70% increase in proton flux (supplemental Fig. S6*A*). The initial alkalinization upon mersalyl addition is consistent with inhibition of coupled P_i/H^+ entry, but the subsequent drop in matrix pH and increased proton flux suggest that the inner membrane has been damaged by mersalyl. We then turned to ion substitution experiments to identify the H^+ transporters involved in the rapid flux of protons across the inner mitochondrial membrane. As shown in supplemental Fig. S6*B*, phosphate removal increased pH_{mito}, whereas phosphate addition decreased pH_{mito}, consistent with coupled P_i/H^+ transport. Conversely, potassium removal (120 mM KCl substituted with 235 mM sucrose) decreased pH_{mito}, whereas the subsequent addition of 50 mM KCl increased pH_{mito} (supplemental Fig. S6*C*). Both effects are consistent with K^+/H^+ exchange because in our short term recordings, mitochondria are not depleted of K^+. A drop in pH_{mito} was also observed in sucrose medium when the bath pH was switched from 7.4 to 7.2 (data not shown). The drop in pH_{mito} could reflect increased K^+/H^+ exchange activity (*i.e.* more K^+ leaving the matrix in exchange for additional external protons). These recordings show that changes in the cytosolic concentration of P_i and K^+ alter the matrix pH in the direction predicted by P_i/H^+ symport and K^+/H^+ exchange.

Together, the pharmacological and ion substitution experiments indicate that the Ca^{2+} uniporter and the Na^+/Ca^{2+} exchanger NCLX do not substantially facilitate the flux of protons into mitochondria during changes in environmental pH. Instead, P_i/H^+ symport and K^+/H^+ exchange activity probably contribute to the rapid adaptation of the mitochondrial matrix pH to changes in cytosolic pH.

DISCUSSION

In this study, we report the first time-resolved quantitative measurements of the changes in ΔpH_m and of the trans-mitochondrial proton fluxes occurring in single living cells during physiological stimulation. The determination of ΔpH_m was permitted by concurrent recordings of mitochondrial and cytosolic pH by combining our new mitochondria-targeted, ratiometric indicator SypHer with the cytosolic dye SNARF. These measurements revealed several novel and unexpected aspects of mitochondrial ionic homeostasis.

First, the resting pH of mitochondria in HeLa cells was unexpectedly low, averaging 7.8 at 25 °C and only 7.6 at 37 °C, a value that increased to 7.8 upon repetitive stimulation with histamine. Previous studies using pH-sensitive GFP mutants reported higher resting pH_{mito} values of ~8–8.2 in HEK-293, Jurkat, and HeLa cells (42, 44, 57). Others, however, reported lower pH_{mito} values, similar to those we report here. A resting pH_{mito} of 7.8 was reported in ECV304 endothelial cells using a mitochondrial EYFP (34) and a pH_{mito} of 7.7 in Madin-Darby canine kidney cells with the ratiometric dye SNARF (58). Recently, we reported a resting pH_{mito} of 7.2 in rat pancreatic β cells that increase to 7.7 upon nutrient stimulation (46). pH_{mito} is an important parameter that determines the ability of mitochondria to fulfill their metabolic and homeostatic functions. pH_{mito} increases early during apoptosis (44), and a low pH_{mito} modulates the opening of the permeability transition pore (59, 60) (reviewed in Ref. 61). In pancreatic β cells, an alkaline pH_{mito} is required for the delayed $[Ca^{2+}]_{cyto}$ that sustains the secretion of insulin in response to glucose (46). Our current measurements with SypHer indicate that the commonly assumed resting pH_{mito} of ~8 probably overestimates typical resting pH_{mito} in HeLa cells and several other cell types. Despite this lower than expected value for pH_{mito}, our ΔpH_m values of 0.5–0.7 pH units derived from static high throughput measurements and 0.2–0.4 pH units derived from dynamic single-cell imaging agree well with the values of ~0.3–0.8 pH units reported in earlier studies with GFP-based probes (34, 43). Because the intermembrane space is 0.7 pH units more acidic than the bulk cytosol (34), the actual ΔpH_m is therefore >1 pH unit. Our data thus indicate that the resting pH_{mito} is quite low in quiescent cells and increases in the wake of agonist-induced Ca^{2+} signaling.

Second, we observed that changes in cytosolic pH were paralleled by changes in mitochondrial pH. Bursts of intracellular proton accumulation, due to the activity of the PMCA (see below), were readily transmitted to the mitochondrial matrix. A similar rapid equilibration of pH_{mito} and pH_{cyto} was reported in MDCK cells during metabolic inhibition and attributed to the proton antiporters of mitochondria (58). Our pH_{mito} recordings from permeabilized cells indicate that the matrix pH is affected both by P_i/H^+ symport and K^+/H^+ exchange activity (supplemental Fig. S6). Because K^+ and P_i are present at high concentration in the matrix and in the cytosol, these two transporters probably contribute to the rapid equilibration of the mitochondrial matrix pH during cytosolic pH excursions. Unfortunately, we could not identify, pharmacologically, a single transporter that could account for the proton fluxes, and only inhibition of the mitochondrial respiratory chain consistently decreased the proton fluxes (by 20–30%) both in intact and permeabilized cells (Fig. 8). However, this inhibition probably reflects the decreased proton-motive force rather than decreased proton permeability. On the one hand, this high permeability of mitochondria to protons appears incompatible with the need for mitochondria to maintain a proton-motive force across their inner membrane. The cytosol to matrix pH gradient is essential for the import and export of a large number of metabolites. It should be kept in mind, however, that respiratory chain complexes cluster in cristae, folds of the inner mitochondrial membrane with restricted diffusional access to the rest of the intermembrane space. It is thus conceivable that H^+ transporters like the Na^+/H^+ exchanger and phosphate/H^+ symporter, whose substrates require easy access to the cytosol, might preferentially localize outside the cristae. Such an arrangement would allow generation of a large pH gradient across of the cristae membrane to power the F_1F_0-ATP synthase while accounting for the relatively high permeability of mitochondria to protons in our experiments. Our quantitative pH data also indicate that, despite the rapid adaptation of pH_{mito} to changes in pH_{cyto}, the matrix remained at all times more alkaline than the cytosol, even during large pH excursions (Fig. 3*C*, *ii*). These data show that mitochondria can maintain a positive cytosol to matrix pH gradient despite large variations in the absolute pH of their matrix and of their surrounding environment. This hitherto unappreciated property might be important to preserve the bioenergetic function of mitochondria in cells exposed to acid or alkaline loads.

Third, we observed unexpected biphasic changes in mitochondrial pH during stimulation of cells with a Ca^{2+}-mobilizing agonist. $[Ca^{2+}]_{cyt}$ elevations were associated with a massive acidification, whereas removal of the agonist increased pH_{mito} above prestimulatory levels. As a result of the overshoot, ΔpH_m strongly depended on prior exposure of cells to exogenous stimuli and increased by ~0.2 pH units after three successive agonist stimulations. This effect was most likely due to the Ca^{2+}-dependent activation of matrix dehydrogenases because matrix alkalinization was also observed in permeabilized cells exposed to 10 μM Ca^{2+}. The Ca^{2+}-induced alkalinization, however, was of smaller amplitude than the acidification evoked by a concomitant decrease in bath pH from 7.4 to 7.2, a condition that mimics the changes occurring in intact cells stimulated with Ca^{2+}-mobilizing agonists. These data indicate that mitochondria slowly alkalinize in response to $[Ca^{2+}]_{cyt}$ elevations but that the alkalinization is masked by a larger and faster acidification as the cytosolic pH drops concomitantly during stimulations with Ca^{2+}-mobilizing agonists.

A prominent mitochondrial acidification was reported in cultured cortical neurons stimulated with glutamate (43) and in endothelial cells stimulated with histamine (62) but not in an earlier pH_{mito} study of HeLa cells (42). We now provide a mechanistic explanation for this $[Ca^{2+}]_{cyt}$-dependent mitochondrial acidification. Three lines of evidence indicate that the PMCA is the source of the acid produced during $[Ca^{2+}]_{cyt}$ elevations: 1) the acidification was proportional to the total calcium load, a kinetic property expected for a Ca^{2+}/H^+ transporter that couples the extrusion of Ca^{2+} ions to proportional entry of protons into cells; 2) the acidification did not require Ca^{2+} uptake or Ca^{2+} release from intracellular stores but was related to plasma membrane Ca^{2+} fluxes; 3) the acidification was prevented by La^{3+} or by alkaline pH_o, two treatments that inhibit the PMCA. The PMCA mediates cytosolic acidification upon toxic stimulation of neurons with domoate (63) and has been postulated to mediate glutamate-induced acidification (43). Our data indicate that the acid generated by the PMCA is transmitted to the mitochondrial matrix. This mechanism might protect cells from excessive Ca^{2+} elevations because an acidic pH_{mito} inhibits the Ca^{2+}-induced opening of the permeability transition

pore (64, 65) and reduces mitochondrial production of potentially toxic radical oxygen species (31). In energized mitochondria, however, an acidic pH has the opposite effect and promotes the opening of the permeability transition pore (60). Thus, whether the transmission of the acid generated by the PMCA to mitochondria has protective or deleterious effects remains to be determined.

Fourth, we report here the first estimates of the pH buffering capacity of mitochondria in intact cells. This parameter was derived from the pH changes evoked by the addition of known concentrations of membrane-permeable weak acid or bases. The determination of β_{mito} enabled us to calculate the fluxes of protons within mitochondria. Our β_{mito} values of 10–18 mM are notably lower than the ~110 mM measured by phosphate-NMR in perfused liver (66) but consistent with values from isolated mitochondria of ~22 nmol/mg protein (67) that translate into a β_{mito} of 11–13 mM, assuming a matrix water volume of 1.6–2.0 μl/mg of protein (68). Our values reflect the intrinsic pH buffering capacity of mitochondria, since our solutions were devoid of bicarbonate. Overall, the pH dependence of the β_{mito} and β_{cyto} had a similar apparent affinity for protons, suggesting that similar molecules buffer protons within the two compartments. This is not too surprising, considering that intrinsic pH buffers (*i.e.* non-bicarbonate) are mainly provided by phosphate groups and side chains of amino acids (69). Importantly, the mitochondrial buffering power dropped rapidly when pH_{mito} increased from 7.6 to 8.0. This suggests that the titrable groups that can bind protons within the matrix of mitochondria have a nearly neutral pK_a. The sharp decrease in β_{mito} at alkaline pH facilitates the generation of a proton gradient as mitochondria become more alkaline, because fewer protons need to be pumped to generate an equivalent change in pH_{mito}. The low buffering capacity of mitochondria thus facilitates the H^+-coupled entry or extrusion of mitochondrial substrates and metabolites during cell activation. On the other hand, the low β_{mito} renders mitochondria vulnerable to surges of cytosolic acid production as a relatively small influx of protons markedly decreases pH_{mito} in alkaline mitochondria. This poor protection was experimentally verified to underlie a larger decrease in pH_{mito} than pH_{cyto} and a consequent decrease of ΔpH_m during Ca^{2+}-induced acidification.

In summary, we show that the mitochondrial pH is not as stable or as alkaline as generally assumed but is dynamically regulated and can vary widely during physiological stimulations. During $[Ca^{2+}]_{cyt}$ elevations, the acid generated by the plasma membrane Ca^{2+} ATPase is transmitted to the mitochondrial matrix and decreases ΔpH_m. The drop in ΔpH_m is due to the reduced buffering power of mitochondria in the alkaline pH range, which by amplifying the changes in pH_{mito} facilitates the generation but also the dissipation of the proton gradient.

Acknowledgments—We thank Drs. Roger Tsien and Amy Palmer for providing the 4mitD3-CPV and YC3.6 constructs, Dr. Vsevolod Belousov for mutagenesis primer sequences, and Dr. Stephan Koënig for technical assistance.

REFERENCES

1. Kroemer, G., Galluzzi, L., and Brenner, C. (2007) *Physiol. Rev.* **87,** 99–163
2. Szabadkai, G., and Duchen, M. R. (2008) *Physiology* **23,** 84–94
3. Hoth, M., Fanger, C. M., and Lewis, R. S. (1997) *J. Cell Biol.* **137,** 633–648
4. Frieden, M., Arnaudeau, S., Castelbou, C., and Demaurex, N. (2005) *J. Biol. Chem.* **280,** 43198–43208
5. Arnaudeau, S., Kelley, W. L., Walsh, J. V., Jr., and Demaurex, N. (2001) *J. Biol. Chem.* **276,** 29430–29439
6. Malli, R., Frieden, M., Osibow, K., Zoratti, C., Mayer, M., Demaurex, N., and Graier, W. F. (2003) *J. Biol. Chem.* **278,** 44769–44779
7. Demaurex, N., Poburko, D., and Frieden, M. (2009) *Biochim. Biophys. Acta* **1787,** 1383–1394
8. Hajnóczky, G., Robb-Gaspers, L. D., Seitz, M. B., and Thomas, A. P. (1995) *Cell* **82,** 415–424
9. Satrústegui, J., Pardo, B., and Del Arco, A. (2007) *Physiol. Rev.* **87,** 29–67
10. Contreras, L., Gomez-Puertas, P., Iijima, M., Kobayashi, K., Saheki, T., and Satrústegui, J. (2007) *J. Biol. Chem.* **282,** 7098–7106
11. Talbot, J., Barrett, J. N., Barrett, E. F., and David, G. (2007) *J. Physiol.* **579,** 783–798
12. Nicholls, D. G. (1974) *Eur. J. Biochem.* **50,** 305–315
13. Mitchell, P. (1961) *Nature* **191,** 144–148
14. Nicholls, D. G. (2008) *Biochim. Biophys. Acta* **1777,** 550–556
15. Wiedenmann, A., Dimroth, P., and von Ballmoos, C. (2008) *Biochim. Biophys. Acta* **1777,** 1301–1310
16. von Ballmoos, C., Wiedenmann, A., and Dimroth, P. (2009) *Annu. Rev. Biochem.* **78,** 649–672
17. Bernardi, P. (1999) *Physiol. Rev.* **79,** 1127–1155
18. Dash, R. K., and Beard, D. A. (2008) *J. Physiol.* **586,** 3267–3285
19. Palty, R., Silverman, W. F., Hershfinkel, M., Caporale, T., Sensi, S. L., Parnis, J., Nolte, C., Fishman, D., Shoshan-Barmatz, V., Herrmann, S., Khananshvili, D., and Sekler, I. (2010) *Proc. Natl. Acad. Sci. U.S.A.* **107,** 436–441
20. Nowikovsky, K., Froschauer, E. M., Zsurka, G., Samaj, J., Reipert, S., Kolisek, M., Wiesenberger, G., and Schweyen, R. J. (2004) *J. Biol. Chem.* **279,** 30307–30315
21. Zotova, L., Aleschko, M., Sponder, G., Baumgartner, R., Reipert, S., Prinz, M., Schweyen, R. J., and Nowikovsky, K. (2010) *J. Biol. Chem.* **285,** 14399–14414
22. Jiang, D., Zhao, L., and Clapham, D. E. (2009) *Science* **326,** 144–147
23. Scarpa, A., and Azzone, G. F. (1970) *Eur. J. Biochem.* **12,** 328–335
24. Rottenberg, H., and Scarpa, A. (1974) *Biochemistry* **13,** 4811–4817
25. Wingrove, D. E., Amatruda, J. M., and Gunter, T. E. (1984) *J. Biol. Chem.* **259,** 9390–9394
26. Bernardi, P., and Azzone, G. F. (1983) *Eur. J. Biochem.* **134,** 377–383
27. Nicholls, D. G., and Chalmers, S. (2004) *J. Bioenerg. Biomembr.* **36,** 277–281
28. Mitchell, P., and Moyle, J. (1969) *Eur. J. Biochem.* **7,** 471–484
29. Chen, L. B. (1988) *Annu. Rev. Cell Biol.* **4,** 155–181
30. Lambert, A. J., and Brand, M. D. (2004) *Biochem. J.* **382,** 511–517
31. Selivanov, V. A., Zeak, J. A., Roca, J., Cascante, M., Trucco, M., and Votyakova, T. V. (2008) *J. Biol. Chem.* **283,** 29292–29300
32. Hoek, J. B., Nicholls, D. G., and Williamson, J. R. (1980) *J. Biol. Chem.* **255,** 1458–1464
33. Brand, M. D., and Felber, S. M. (1984) *Biochem. J.* **217,** 453–459
34. Porcelli, A. M., Ghelli, A., Zanna, C., Pinton, P., Rizzuto, R., and Rugolo, M. (2005) *Biochem. Biophys. Res. Commun.* **326,** 799–804
35. Halestrap, A. P., and Pasdois, P. (2009) *Biochim. Biophys. Acta* **1787,** 1402–1415
36. Brand, M. D., and Esteves, T. C. (2005) *Cell Metab.* **2,** 85–93
37. Jousset, H., Frieden, M., and Demaurex, N. (2007) *J. Biol. Chem.* **282,** 11456–11464
38. Belousov, V. V., Fradkov, A. F., Lukyanov, K. A., Staroverov, D. B., Shakhbazov, K. S., Terskikh, A. V., and Lukyanov, S. (2006) *Nat. Methods* **3,** 281–286
39. Palmer, A. E., Jin, C., Reed, J. C., and Tsien, R. Y. (2004) *Proc. Natl. Acad. Sci. U.S.A.* **101,** 17404–17409
40. De Marchi, U., Campello, S., Szabò, I., Tombola, F., Martinou, J. C., and

Zoratti, M. (2004) *J. Biol. Chem.* **279,** 37415–37422
41. Roos, A., and Boron, W. F. (1981) *Physiol. Rev.* **61,** 296–434
42. Abad, M. F., Di Benedetto, G., Magalhães, P. J., Filippin, L., and Pozzan, T. (2004) *J. Biol. Chem.* **279,** 11521–11529
43. Bolshakov, A. P., Mikhailova, M. M., Szabadkai, G., Pinelis, V. G., Brustovetsky, N., Rizzuto, R., and Khodorov, B. I. (2008) *Cell Calcium* **43,** 602–614
44. Matsuyama, S., Llopis, J., Deveraux, Q. L., Tsien, R. Y., and Reed, J. C. (2000) *Nat. Cell Biol.* **2,** 318–325
45. Scaduto, R. C., Jr., and Grotyohann, L. W. (1999) *Biophys. J.* **76,** 469–477
46. Wiederkehr, A., Park, K. S., Dupont, O., Demaurex, N., Pozzan, T., Cline, G. W., and Wollheim, C. B. (2009) *EMBO J.* **28,** 417–428
47. Trenker, M., Malli, R., Fertschai, I., Levak-Frank, S., and Graier, W. F. (2007) *Nat. Cell Biol.* **9,** 445–452
48. Frieden, M., James, D., Castelbou, C., Danckaert, A., Martinou, J. C., and Demaurex, N. (2004) *J. Biol. Chem.* **279,** 22704–22714
49. Niggli, V., Sigel, E., and Carafoli, E. (1982) *J. Biol. Chem.* **257,** 2350–2356
50. Thomas, R. C. (2009) *J. Physiol.* **587,** 315–327
51. Niggli, V., and Sigel, E. (2008) *Trends Biochem. Sci.* **33,** 156–160
52. Brini, M., and Carafoli, E. (2009) *Physiol. Rev.* **89,** 1341–1378
53. Carafoli, E. (1992) *J. Biol. Chem.* **267,** 2115–2118
54. Gover, T. D., Moreira, T. H., Kao, J. P., and Weinreich, D. (2007) *Cell Calcium* **41,** 389–396
55. Vaughan-Jones, R. D., and Wu, M. L. (1990) *J. Physiol.* **425,** 429–448
56. Santo-Domingo, J., and Demaurex, N. (2010) *Biochim. Biophys. Acta* **1797,** 907–912
57. Llopis, J., McCaffery, J. M., Miyawaki, A., Farquhar, M. G., and Tsien, R. Y. (1998) *Proc. Natl. Acad. Sci. U.S.A.* **95,** 6803–6808
58. Balut, C., vandeVen, M., Despa, S., Lambrichts, I., Ameloot, M., Steels, P., and Smets, I. (2008) *Kidney Int.* **73,** 226–232
59. Bernardi, P., Vassanelli, S., Veronese, P., Colonna, R., Szabó, I., and Zoratti, M. (1992) *J. Biol. Chem.* **267,** 2934–2939
60. Kristian, T., Bernardi, P., and Siesjö, B. K. (2001) *J. Neurotrauma* **18,** 1059–1074
61. Halestrap, A. P. (2009) *J. Mol. Cell Cardiol.* **46,** 821–831
62. Malli, R., Frieden, M., Osibow, K., and Graier, W. F. (2003) *J. Biol. Chem.* **278,** 10807–10815
63. Vale-González, C., Alfonso, A., Suñol, C., Vieytes, M. R., and Botana, L. M. (2006) *J. Neurosci. Res.* **84,** 326–337
64. Petronilli, V., Cola, C., and Bernardi, P. (1993) *J. Biol. Chem.* **268,** 1011–1016
65. Bernardi, P. (1992) *J. Biol. Chem.* **267,** 8834–8839
66. Durand, T., Delmas-Beauvieux, M. C., Canioni, P., and Gallis, J. L. (1999) *Cryobiology* **38,** 68–80
67. Mitchell, P., and Moyle, J. (1965) *Nature* **208,** 147–151
68. Bednarczyk, P., Barker, G. D., and Halestrap, A. P. (2008) *Biochim. Biophys. Acta* **1777,** 540–548
69. Casey, J. R., Grinstein, S., and Orlowski, J. (2010) *Nat. Rev. Mol. Cell Biol.* **11,** 50–61